

Auriferous Sulfides from the Chah-Bagh Gold Occurrence, Muteh Mining District

H. Kouhestani, E. Rastad,* and N. Rashidnejad Omran

Department of Geology, Faculty of Basic Sciences, Tarbiat Modarres University, Tehran 14115-175, Islamic Republic of Iran

Abstract

The Chah-Bagh gold occurrence is located in Muteh mining district, in the central part of the Sanandaj-Sirjan zone. Gold mineralization occurs in ductile to ductile-brittle shear zones and is comparable with orogenic gold deposits. Silicification and sulfidization are the most important hydrothermal alteration features in the inner parts of altered shear zones and coincide most closely with the ore-bearing zones. Principal ore minerals are pyrite, chalcopyrite, arsenopyrite and native silver. Silver commonly occurs both as native Ag grains (ca. 5 μm in diameter) intimately associated with siliceous gangue and as invisible silver within sulfides. The maximum concentration of invisible silver occurs in chalcopyrite. Although native gold was not identified in the siliceous gangue and in the sulfide minerals and their alteration products, electron microprobe analyses confirmed the occurrence of invisible gold within sulfides. Two phases of gold mineralization occurred in the Chah-Bagh area: 1- invisible gold within coarse-grained sulfides (pyrite and chalcopyrite); 2- invisible gold (the main phase) within fine-grained sulfides (pyrite and chalcopyrite). Evidently, the precipitation of gold was an integral part of the hydrothermal alteration system and was associated with sulfide minerals. Although electron microprobe analyses of auriferous sulfide indicated the presence of gold in sufficient quantities to explain the bulk gold concentrations, native gold has not been detected in our polished sections.

Keywords: Invisible gold; Auriferous sulfides; Ore minerals; Chah-Bagh; Muteh

Introduction

The Chah-Bagh gold occurrence of the Muteh mining district is located in the central part of the Sanandaj-Sirjan metamorphosed zone of the Zagros orogenic belt (Fig. 1), about 270 km SW of Tehran. The

Zagros orogenic belt was formed by collision between the Afro-Arabian continent and the Iranian microcontinent in the Late Cretaceous-Tertiary times [1-3]. This orogenic belt includes four parallel structural zones, from northeast to southwest (Fig. 1): 1) Urumieh-Dokhtar Magmatic Arc, 2) Sanandaj-Sirjan Zone, 3)

* Corresponding author, Tel.: +98(21)82883436, Fax: +98(21)82883436, E-mail: rastad@modares.ac.ir

Zagros Fold-and-Thrust Belt, and 4) Mesopotamian-Persian Gulf foreland basin [1,4].

There are ten gold deposits and occurrences in the Muteh mining district (Fig. 2). Unlike other mineralized areas in the district which are localized in brittle shear zones [5-7], the gold mineralization at Chah-Bagh occurs in ductile to ductile-brittle shear zones [8]. In many ways Chah-Bagh appears to be similar to the classic orogenic gold deposits. This type of gold deposits, which formed as a direct consequence of mountain-building processes in Precambrian and Phanerozoic terranes [9-11] constitute an economically important class of auriferous deposits [12] and have a wide distribution throughout the world [13-16]. This type of mineralization has recently been identified in Iran, mainly in the Sanandaj-Sirjan deformation zone. Examples include Kervian in the northwestern part [17], Muteh in the central part [7,8] and Zartorosht in the southeastern part [18] of the Sanandaj-Sirjan zone (Fig. 1).

In recent years, the Chah-Bagh gold occurrence has been studied in detail including petrography, petrology, deformation analysis, geochemistry and genesis of gold mineralization [7, 8, 19-22]. In this paper, the textures, mineralogy and geochemistry of the ore minerals and their paragenetic sequences are presented.

Geological Setting and Mineralization

The main lithologic units at the Chah-Bagh gold occurrence consist of a suite of NE-SW trending, metamorphosed volcanic and volcano-sedimentary rocks (Fig. 3). These rocks, which are part of a metamorphic complex, are Devonian or pre-Devonian in age [7]. They underwent greenschist- to lower amphibolite grades of metamorphism, associated with Mesozoic orogenic events. They are composed of chlorite-actinolite schist, felsic schist, metarhyolite, mylonitized rhyolite, and metabasalt. Mafic sills and dikes are widespread in the western and northern parts of the district. A mylonitized, coarse-grained granite occurring to the east of the Kal-shour valley (Fig. 3), is the only intrusive body in the Chah-Bagh area. It covers an area of 8-9 km² and is localized along a ductile shear zone [8]. Quartz, Na-plagioclase, and biotite are the principal minerals. Based on the timing of granite emplacement in the north of Muteh [19], this granite was emplaced probably during the Late Cretaceous.

Several intense deformation phases in the area led to generation of different fabrics and structures. Seddigh [23], Saba [24] and Hasani *et al.* [25] identified three deformation stages (D1-D3) in the area, of which D2 is the most important phase forming a WNW-trending (N280-N290°), reverse, dextral, ductile shear zone 3 km

long and 2 km wide. Mylonitic foliation (at various scales), penetrative foliation (S2), large-scale stretching/mineral lineations, and F2 folds were developed during D2 deformation stage. According to Valizadeh and Cantagrel [26], D2 deformation is constrained to the Late Cretaceous by a suite of post-tectonic Paleocene plutons that are widely developed in the northwestern Sanandaj-Sirjan Zone. This deformation is the result of the oblique collision of the Afro-Arabian continent with the southwestern part of central Iran (Sanandaj-Sirjan Zone) during the Late Cretaceous [1]. Most of the gold mineralization occurred contemporaneous with this stage. The ⁴⁰Ar/³⁹Ar dating by Moritz *et al.* [27] suggest a Cretaceous to early Tertiary metamorphic, magmatic, and deformation history of the complex hosting the Muteh gold deposit.

Hydrothermal alteration phases include sericite, epidote, quartz, and sulfide minerals. The intensity of alteration is variable and ranges from weak to pervasive. Silicification and sulfidation of wall rocks are usually observed in the inner parts of altered shear zones and coincide most closely with the ore-bearing zones [8]. Silica, in the form of quartz, is also developed as laminated veins, veinlets, and quartz lenses spatially associated with the most intensely deformed rocks, and stands as hard, resistant outcrops. Sulfide alteration assemblages are present in the deformational zones and usually coincide with the mineralized zones. The principal sulfide phases are pyrite, chalcopyrite and arsenopyrite. Moritz and Ghazban [5,6], Rashidnejad Omran [7] and Moritz *et al.* [27] reported carbonate alteration as quartz-carbonate-pyrite veins and as carbonate veinlets in the Muteh brittle shear zones.

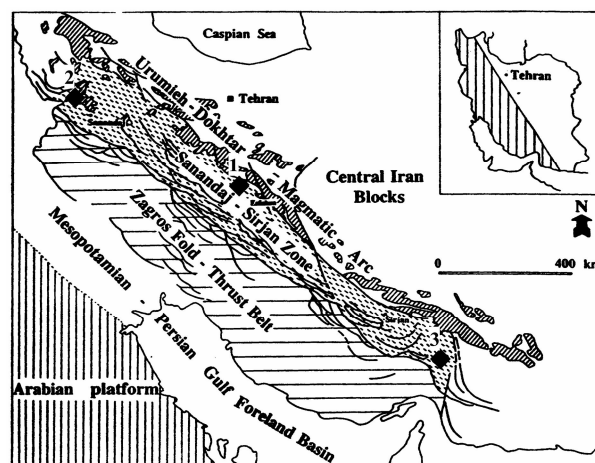


Figure 1. Tectonic zones of the Zagros Orogenic belt [54] and location of the Muteh mining district (1), Kervian gold occurrence (2) and Zartorosht gold deposit (3) along the Sanandaj-Sirjan zone.

Auriferous Sulfides from the Chah-Bagh Gold Occurrence, Muteh Mining District

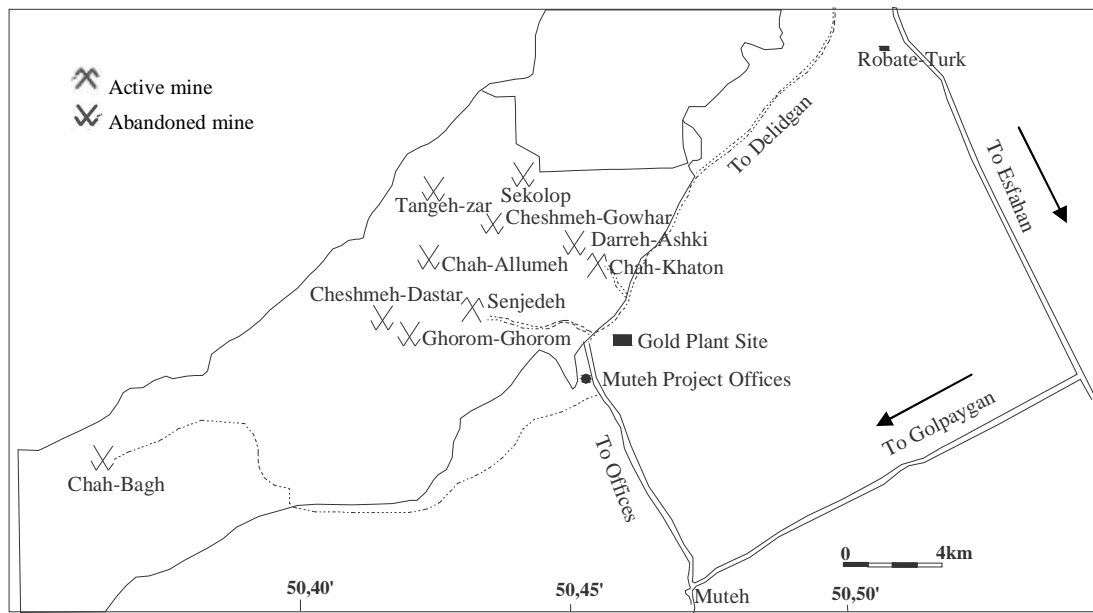


Figure 2. Location map of the Chah-Bagh and other gold deposits and occurrences in the Muteh mining district [8].

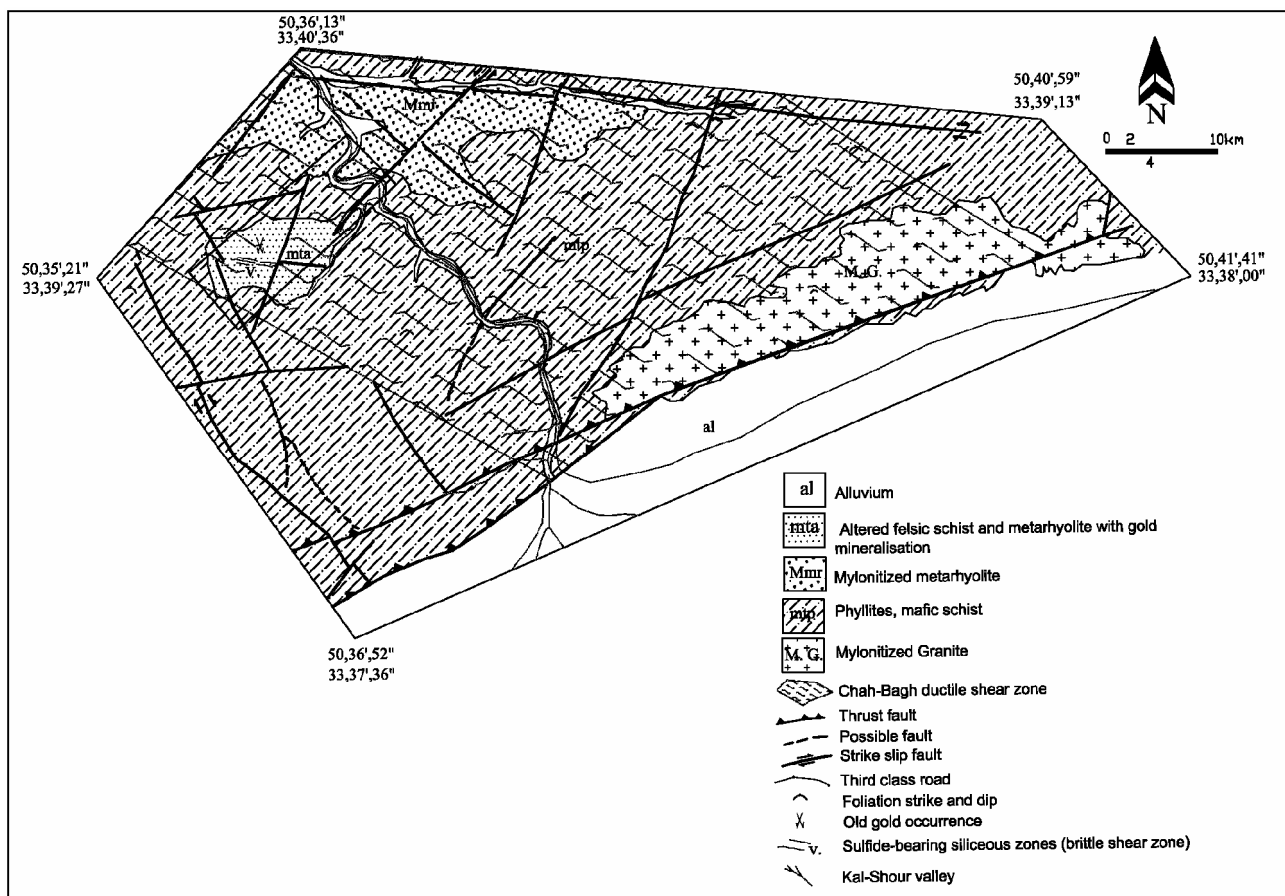


Figure 3. Geological map of the Chah-Bagh area and location of the Chah-Bagh gold occurrence [8].

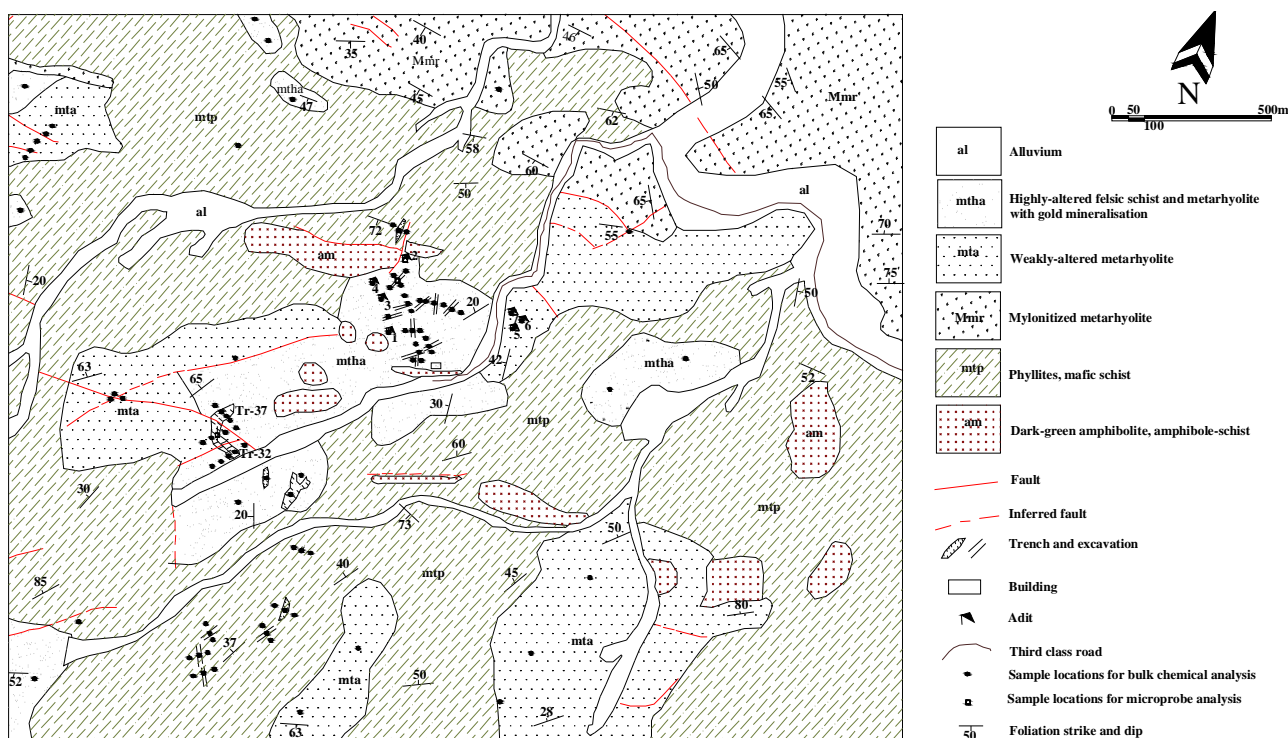


Figure 4. Geological map and location of tunnels, trenches and samples at the Chah-Bagh gold occurrence [8].

The Chah-Bagh gold occurrence is located in a W-NW-trending (N 280-290), reverse, dextral, ductile shear zone [8]. Both ductile and brittle gold-bearing structures have been identified in the Chah-Bagh area [8]. The largest gold resource occurs as a steep NE-dipping (N60-80E) and NW striking lenticular body, 1-km-long and 60-m-wide in the NW-trending (N40-50W) ductile shear zone. In addition to the main gold resource in the ductilely deformed rocks, brittle styles of gold mineralization, similar to other deposits in the Muteh mining area [5,6,27], are also observed at the Chah-Bagh as gold-bearing sulfide-rich quartz veins along N40W-trending, NE-dipping extensional normal faults. The host rocks are composed of intensely altered and deformed felsic schist and metarhyolite, associated with chlorite-actinolite schists.

Sampling and Analytical Methods

Detailed field work has been carried out at different scales in the Chah-Bagh area. The sampling was carried out parallel and perpendicular to the general foliation trend (Fig. 4). About 50 polished slabs, polished thin sections and thin sections from mineralized and altered zones were studied by conventional petrographic and mineralogical methods at the Department of Geology,

Tarbiat Modarres University Tehran. Detailed petrographic and mineralogical descriptions are presented in Kouhestani [8]. In addition, 3 polished thin sections were investigated for chemical composition of the sulfide minerals by quantitative electron microprobe analyses (EMPA).

The compositions of selected minerals were determined on carbon-coated polished thin sections using a CAMECA SX100 probe at the Iranian Mineral Deposits Processing Research Center. A beam current of 20 nA at an accelerating voltage of 20 kV and a beam size of 3 μm were used. The counting time was 20s, the standard used was pure Au metal (99.99 percent) and the detection limit for gold was 100 ppm. The measured elements were Au, Ag, As, Sb, Fe, Cu, Zn, Pb, Te and S. The chemical compositions of sulfides are shown in Table 1.

Ore Mineralogy and Mineral Chemistry

The principal ore minerals observed in the mineralized zones are pyrite, arsenopyrite, chalcopyrite and native silver. They occur as disseminated grains in deformed host-rocks and occasionally parallel to foliations.

Pyrite is the most abundant sulfide (nearly 90

Auriferous Sulfides from the Chah-Bagh Gold Occurrence, Muteh Mining District

Table 1. Mineral chemistry of selected sulfides from electron probe microanalyses (all elements are given in wt percent). Asp-arsenopyrite; Py I- pyrite type I; Py II- pyrite type II; Cpy I- chalcopyrite type I; Cpy II- chalcopyrite type II

Sample No.	Name	S	Fe	Cu	Zn	As	Ag	Sb	Te	Au	Total
ch10-d 1 / 1	Py I	51.26	45.89	0.02	0.08	0.27	0.03	0.00	0.00	0.06	97.61
ch10-d 3 / 1	Py I	53.44	47.11	0.00	0.00	0.53	0.00	0.00	0.00	0.06	101.15
ch10-d1-1 / 1	Py I	53.22	47.20	0.02	0.00	0.28	0.00	0.00	0.03	0.00	100.74
ch10-d1-2 / 1	Py I	53.11	46.69	0.00	0.03	0.31	0.01	0.06	0.01	0.00	100.22
ch10-e 2 / 1	Py I	52.27	47.67	0.04	0.0	0.31	0.00	0.00	0.00	0.07	100.35
ch10-g1-2 / 1	Py I	51.80	47.29	0.02	0.02	0.41	0.00	0.00	0.00	0.00	99.54
ch33-j1 / 1	Py I	53.02	47.80	0.01	0.05	0.14	0.00	0.01	0.00	0.00	101.02
ch33-j2 / 1	Py I	50.07	46.88	0.00	0.00	0.05	0.09	0.02	0.00	0.03	97.15
ch33-j3 / 1	Py I	54.08	46.89	0.00	0.00	0.41	0.00	0.03	0.00	0.02	101.43
ch33-j1-2 / 1	Py I	50.07	46.22	0.00	0.02	0.39	0.04	0.03	0.00	0.06	96.83
ch38(4)-1 / 1	Py I	53.61	47.17	0.02	0.00	0.19	0.10	0.00	0.00	0.04	101.13
ch38(4)-2 / 1	Py I	52.39	47.14	0.00	0.02	0.21	0.03	0.00	0.00	0.00	99.79
ch10-f 1 / 1	Py II	51.31	46.36	0.00	0.00	0.30	0.05	0.00	0.01	0.01	98.04
ch10-f 2 / 1	Py II	51.73	46.91	0.00	0.05	0.29	0.00	0.00	0.00	0.25	99.23
ch10-h 1 / 1	Py II	52.20	47.04	0.02	0.04	0.37	0.00	0.00	0.05	0.00	99.72
ch10-h 2 / 1	Py II	52.49	47.06	0.00	0.00	0.31	0.00	0.04	0.00	0.05	99.94
ch10-i 1 / 1	Py II	52.60	45.60	0.00	0.04	0.47	0.10	0.00	0.00	0.06	98.86
ch10-i 3 / 1	Py II	52.86	47.71	0.02	0.00	0.65	0.00	0.03	0.01	0.18	101.46
ch10-i1-1 / 1	Py II	51.64	46.83	0.04	0.07	0.57	0.00	0.01	0.00	0.19	99.35
ch10-i1-2 / 1	Py II	53.82	47.29	0.13	0.04	0.19	0.00	0.00	0.00	0.00	101.46
ch10-j 1 / 1	Py II	52.72	46.35	0.00	0.00	0.30	0.04	0.00	0.00	0.08	99.50
ch10-j 3 / 1	Py II	50.03	45.11	0.06	0.03	0.55	0.04	0.02	0.03	0.00	95.87
ch33-f 1 / 1	Py II	51.88	45.97	0.03	0.00	0.08	0.02	0.03	0.00	0.00	98.02
ch38(2)-1 / 1	Cpy I	35.16	30.58	34.06	0.00	0.00	0.00	0.00	0.00	0.00	99.80
ch38(2)-2 / 1	Cpy I	35.30	30.50	33.82	0.05	0.05	0.00	0.01	0.00	0.17	99.89
ch38(3)-1 / 1	Cpy I	34.64	29.81	33.28	0.03	0.07	0.08	0.00	0.00	0.00	97.93
ch38(3)-2 / 1	Cpy I	35.09	29.47	33.98	0.11	0.04	0.03	0.02	0.01	0.10	98.84
ch38-a-1 / 1	Cpy I	34.29	29.06	34.12	0.01	0.07	0.14	0.00	0.00	0.07	97.76
ch38-a1-2 / 1	Cpy I	33.51	24.57	30.50	0.16	10.78	0.01	0.00	0.00	0.22	99.74
ch10-c 1 / 1	Cpy II	32.36	29.51	33.59	0.01	0.06	0.01	0.01	0.02	0.07	95.65
ch10-c 2 / 1	Cpy II	33.73	29.88	34.24	0.04	0.01	0.00	0.00	0.07	0.46	98.43
ch10c-1-1 / 1	Cpy II	34.60	29.73	34.04	0.02	0.11	0.02	0.08	0.02	0.00	98.62
ch33-e-2 / 1	Cpy II	34.47	29.12	35.19	0.02	0.00	0.10	0.04	0.00	0.00	98.93
ch33-e1-2 / 1	Cpy II	35.10	24.33	40.22	0.01	0.04	0.05	0.00	0.00	0.00	99.75
ch33-g4-2 / 1	Asp	24.90	35.76	0.05	0.00	35.28	0.04	0.00	0.06	0.00	96.09
ch33-g4-3 / 1	Asp	20.04	35.56	0.14	0.00	42.73	0.04	0.00	0.00	0.00	98.51
ch33-i 1 / 1	Asp	16.30	33.92	0.03	0.07	46.24	0.00	0.00	0.00	0.13	96.70
ch33-i1-2 / 1	Asp	22.06	36.30	0.09	0.04	42.97	0.07	0.00	0.01	0.00	101.55
ch33-i3-1 / 1	Asp	22.69	35.89	0.00	0.00	42.54	0.07	0.05	0.00	0.00	101.25

percent of sulfide minerals), and its abundance increases toward the center of the shear zone. It generally occurs as coarse euhedral to fine anhedral grains and coexists with quartz and other sulfides. Two types of pyrite were recognized, mainly based on structural and textural

relationships. The earlier (pyrite I) occurs as euhedral coarse grains, up to 2 mm in diameter, with characteristic elongated and laminated shape. These pyrite grains are parallel to the mylonitic foliation (Fig. 5). They are deformed, folded and elongated perpendi-

cular to the maximum stress axis or show σ -type mantle-porphyroblasts shape (Fig. 6). Alteration of pyrite to Fe-hydroxide is common. Some euhedral pyrite grains are fractured and brecciated. This fracturing may be attributed to a later deformational event.

Electron microprobe analyses of this type of pyrite indicate the presence of As, Ag, Cu, Zn, Sb and Te as common trace elements. Arsenic is the most abundant trace element and its content generally increases from core to rim (Table 1), so that the highest As values (up to 0.53 wt percent) are found in the margins. This pyrite is directly associated with gold mineralization [8].

The second type of pyrite (pyrite II) is characterized by disseminations and veinlets of fine-grained anhedral to subhedral crystals, up to 100 μm in diameter (Fig. 7). Oriented pyrites were rarely observed. The pyrite grains have no deformation signatures, and probably were deposited late in the hydrothermal and deformational history of the Chah-Bagh area. On the basis of electron microprobe analyses, trace elements include As, Ag, Cu, Zn, Sb and Te. In this type of pyrite, the As concentration reaches up to 0.65 wt percent. Electron microprobe analyses of this type of pyrite indicate higher average gold concentrations compared to pyrite-I.

The occurrence of As-rich pyrites has been reported by many authors in gold deposits [28-32]. Although it is unclear how much As can be incorporated into the structure of pyrite [33], it should be noted that a maximum value of only 0.53 wt percent As in pyrite was determined in the dry experiments of Clark [34]. More recent studies by Fleet and Mumin [35] yielded up to 9.3 wt percent As in pyrite. Fleet *et al.* [30] and Dickson *et al.* [36] concluded that As is incorporated as a metastable solid solution in pyrite. Ballantyne and Moore [32], Fleet *et al.* [30] and Sibson *et al.* [37] supposed an episodic flow of hydrothermal fluid during mineralization or a redox disequilibrium reaction between the adjacent As-bearing ore fluid and crystallizing pyrites, which caused occurrence of oscillatory composition of As in As-rich pyrite. Yardley *et al.* [38], however, gave another plausible mechanism attributed to the As changes in the activity of the involved species in the fluid, as a consequence of rapid changes in the fluid oxidation state. Rytuba [31] and Dill *et al.* [29] stated that As-rich pyrites were the result of As coating on pyrite surfaces. At the Chah-Bagh gold occurrence, electron microprobe analyses and textural relationship of the As-rich pyrites suggest the metastable solid solution deposition and/or submicron-size particles of As for the occurrence of As-rich pyrites. Asadi *et al.* [39,40] have also reported such phenomenon in the Zarshuran Carlin-type gold deposit for As-rich pyrites and other sulfide minerals.



Figure 5. Oxidized pyrites (Py I) parallel to mylonitic foliation in intensely deformed (ultramylonite) felsic schist.

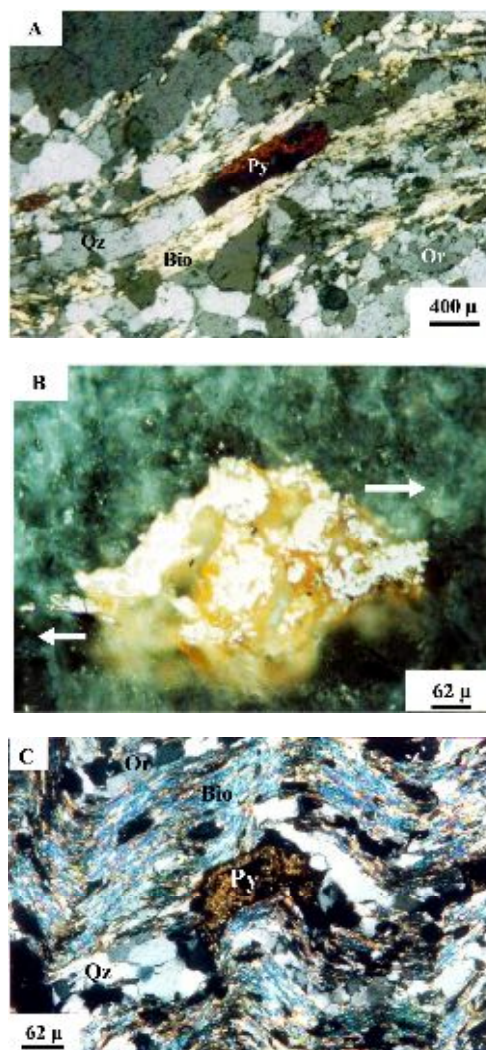


Figure 6. Photomicrographs of pyrite (Py I). A: a deformed and elongated euhedral oxidized pyrite perpendicular to the maximum stress axis, and parallel to mylonitic foliation, transmitting light, XPL. B: a deformed and oxidized pyrite with σ -type mantle-porphyroblast shape, reflected light, oil, PPL. C: a deformed and folded oxidized pyrite parallel to mylonitic foliation, transmitting light, XPL. Qz: quartz, Or: orthoclase, Bio: biotite.

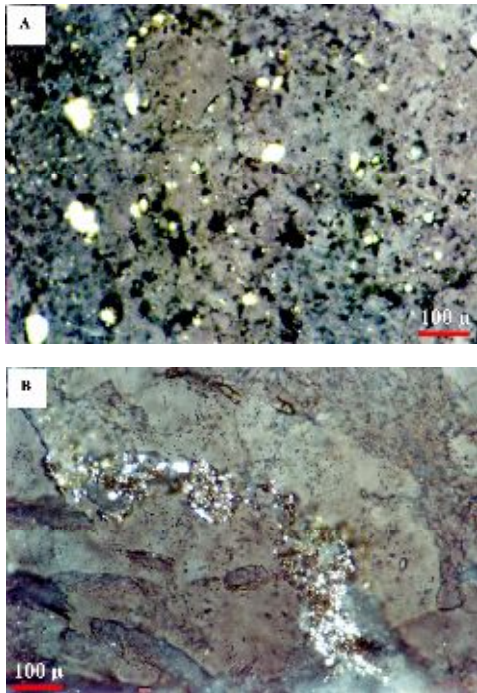


Figure 7. Photomicrographs of disseminated (A) and veinlet (B) fine-grained anhedral to subhedral pyrite (Py II) in inner parts of altered zones, reflected light, PPL.

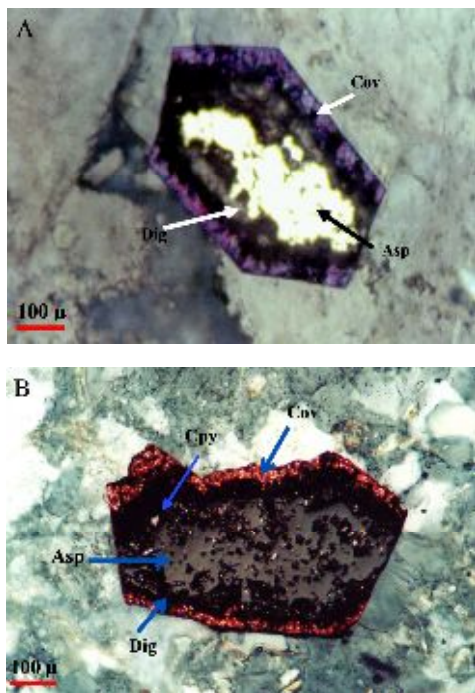


Figure 8. Photomicrographs of euhedral (A) and subhedral (B) arsenopyrite grains with alteration of covellite and digenite at the grain margins. Chalcopyrite inclusions (Cpy II) are observed in B. A: reflected light, oil, PPL and B: reflected light, oil, XPL. Asp: arsenopyrite, Cpy: chalcopyrite, Dig: digenite, Cov: covellite.

Arsenopyrite, the most abundant ore mineral after pyrite in the Chah-Bagh, is generally present as coarse (4 mm) euhedral to subhedral and anhedral isolated grains (Fig. 8) associated with pyrite and quartz. In places, arsenopyrite occurs as elongated aggregates (Fig. 9). Chalcopyrite inclusions (2-3 µm) are occasionally observed in arsenopyrite (Fig. 8). In some places, there is an irregular mutual boundary between subhedral arsenopyrite and euhedral pyrite grains. This phenomenon indicates a simultaneous growth of pyrite and arsenopyrite from the same ore fluid [41,42]. Electron microprobe analyses indicate substantial amounts of Cu in arsenopyrite. High levels of Cu (up to 0.14 percent) were observed in growth zones along the margins of some arsenopyrites. Interaction of arsenopyrite and chalcopyrite with supergen Cu-rich fluids resulted in the formation of covellite and digenite at the grain margins (Fig. 10). Other detectable trace elements present in the arsenopyrite are Ag, Zn, Sb and Te. Rarely does arsenopyrite show detectable amounts of gold by electron probe microanalyses.

Chalcopyrite occurs locally and coexists with quartz and other sulfides. It occurs as coarse to fine subhedral and anhedral grains, and is more abundant in the center of altered shear zones. Alteration of chalcopyrite to covellite and digenite at grain margins is commonly observed. Two types of chalcopyrite were distinguished based on the textural relationships. The earlier (chalcopyrite I) occurs as coarse subhedral to anhedral grains, up to 5 mm in diameter. This type of chalcopyrite occurs as isolated grains in siliceous gangue and in close association with pyrite I (Fig. 11). The second type is common as disseminations and veinlets of fine anhedral to subhedral grains, up to 150 µm in diameter, in close association with fine-grained pyrite (Py II) in the siliceous gangue (Fig. 12), and is locally abundant (up to 1 wt percent). This type is also observed as inclusions (2-3 µm) in arsenopyrite (Fig. 8). Electron microprobe analyses indicated variable contents of As, Ag, Zn, Sb and Te in both types of chalcopyrite. High levels of As, up to 10.78 wt percent, and Ag, up to 0.14 wt percent, were detected in some chalcopyrite grains. These chalcopyrites are directly associated with gold mineralization as shown by electron probe microanalyses [8].

Silver commonly occurs as native Ag grains, <5 µm in size, intimately associated with quartz (Fig. 13), and as invisible Ag within sulfide minerals. High levels of Ag, up to 0.14 wt percent and up to 0.10 wt percent, were observed in chalcopyrite I and chalcopyrite II, respectively.

Gold at Chah-Bagh is detectable only by quantitative electron microprobe analyses and bulk chemical

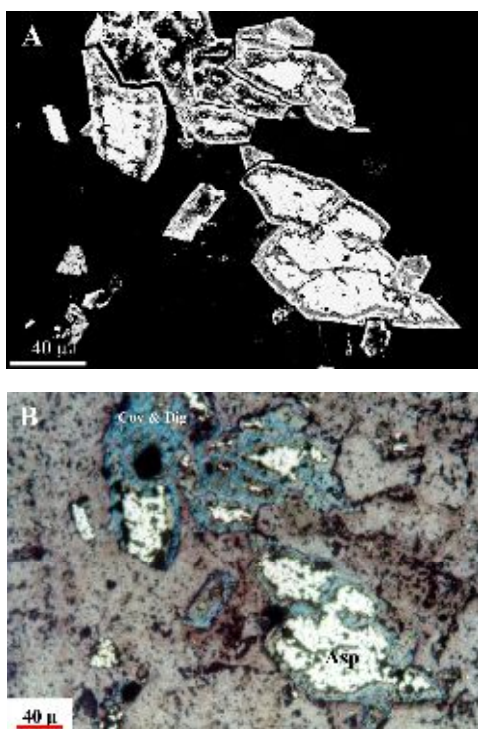


Figure 9. Back-scattered electron (A) and reflected light, oil, PPL (B) images showing arsenopyrite aggregates in deformed and altered rocks from brittle shear zone.

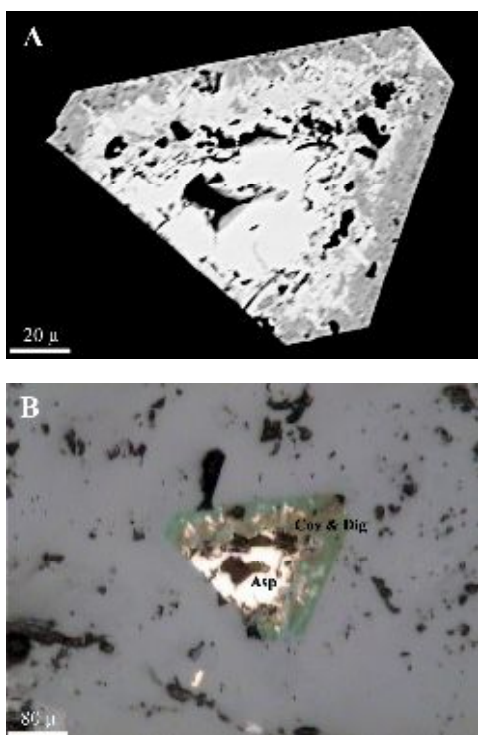


Figure 10. Back-scattered electron (A) and reflected light, oil, PPL (B) images showing arsenopyrite (Asp) replaced by covellite (Cov) and digenite (Dig).

analyses. Examination of samples by high-resolution optical microscopy and electron microprobe analyses, including those found by chemical analyses to have high gold concentrations (in the order of 1.48 to 13.3 ppm), failed to reveal any native gold associated with quartz and altered sulfide grains. The absence of visible gold, coupled with the high concentrations of gold in the mineralized rocks, lends credence to the occurrence of invisible gold at Chah-Bagh [*i.e.* 43-46]. Quantitative point analyses indicate that invisible gold is mainly present in sulfide minerals. The invisible gold appears to be associated with both types of pyrite and chalcopyrite. In bulk ore analyses, gold shows positive correlation with arsenic [8]; however, quantitative electron microprobe analyses of several arsenopyrite grains failed to confirm this relationship which is probably due to the lack of consistency in electron microprobe analyses of arsenopyrite.

A substantial quantity of gold is contained in the sulfides, with concentrations ranging from 0.01 to 0.46 wt percent. The concentration of gold is extremely high in pyrite I (up to 0.07 wt percent), pyrite II (up to 0.25 wt percent), chalcopyrite I (up to 0.22 wt percent) and chalcopyrite II (up to 0.46 wt percent). Gold is mainly concentrated in the inner parts of alteration zones. Bulk chemical analyses of mineralized host rock [8] also yielded high gold grades (up to 13.3 and 7 ppm) in samples containing disseminated and anhedral fine grains of pyrite and chalcopyrite.

The electron microprobe analyses of auriferous sulfide minerals show that gold is present in quantities sufficient to explain the bulk gold grades established by exploration trenches and tunnels. However, it is likely that native gold occurs at Chah-Bagh with irregular distribution or as submicroscopic metallic particles, which may not have been present in our polished sections. This relationship has similarities with other orogenic gold deposits, *i.e.* Kervian [17] and Zartorosht [18], in the Sanandaj-Sirjan zone. The similarities include the presence of invisible gold associated with disseminated fine-grained anhedral pyrite, and the positive correlation of gold with the sulfide contents, particularly with fine-grained anhedral pyrite. Asadi *et al.* [39,40] and Mehrabi *et al.* [47] have also established the presence of invisible gold in anhedral pyrite and other sulfide minerals in the Zarshuran Carlin-type gold deposit.

Quartz is the most common gangue mineral in association with sulfide minerals. Microscopic studies indicate three distinct types of quartz: pre-deformation quartz, early hydrothermal quartz, and late sulfide-bearing quartz (Fig. 14). The pre-deformational quartz (quartz I) existed before deformation and is not an

alteration product. It appears as porphyroblasts (about 2 mm) and is abundant in deformed rocks (Fig. 14). It usually contains numerous small fluid inclusions and has a dark appearance under the microscope. The quartz displays undulose extinction, porphyroblastic mortar texture, and recrystallization features. Recrystallization appears along the borders of crushed quartz grains. The early hydrothermal quartz (quartz II) (0.15-0.25 mm in diameter) has a clear appearance, occurring both in veinlets and in granular aggregates (Fig. 14). Some grains may be deformed. The veinlets and the granular quartz are usually cut by younger sulfide-bearing veinlets. The quartz grains have been formed during dynamic recrystallization through grain boundary migration and sub-grain rotation. The late sulfide-bearing hydrothermal quartz (quartz III) appears as dark fine grains (<200 μ) under the microscope and characteristically hosts sulfide minerals (Fig. 14). This type of quartz occurs in fractures that cut the two earlier quartz stages. Optical microscopic studies have not proved the association of native gold with the quartz.

Paragenetic Sequences

Mineral paragenesis has been established by studying about 50 thin, polished thin and polished sections, and electron microprobe analyses. The mineralogy, textural association, deformation parameters and geochemistry of ore minerals indicates two stages of paragenesis (Fig. 15) for the Chah-Bagh occurrence:

Stage I is characterized by silica (quartz II) without any evidence of sulfide mineralization. Microscopic studies and electron microprobe analyses found no evidence of gold mineralization associated with this stage.

Stage II is characterized by dominant siliceous (quartz III) and sulfide (I and II) alteration. Based on textural association of alteration minerals, microscopic studies and electron microprobe analyses, this stage can be divided into two sub-stages:

Sub-stage I includes sulfide mineralization (type I) and contains the first phase of gold mineralization. The sulfides formed during this sub-stage, occurred either as disseminated grains or along fractures or grain boundaries in quartz I and II, and other rock-forming minerals. Microfractures in these crystals were cemented by the second type of sulfides and associated quartz. These phenomena indicate that this type of sulfide was formed in the early stage of hydrothermal alteration, but after the early hydrothermal quartz (quartz II). Coarse-grained euhedral pyrite, arsenopyrite and chalcopyrite are the principal sulfide minerals. Gold occurs as invisible Au in sulfide minerals (pyrite and

chalcopyrite), but silver was found both as invisible Ag in sulfide minerals as well as native Ag intimately associated with quartz.

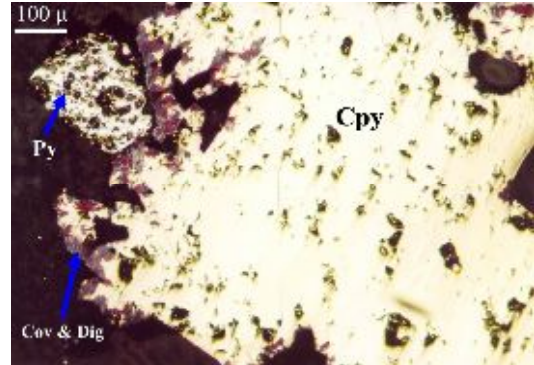


Figure 11. Photomicrograph of chalcopyrite (Cpy I) in close association with grains of pyrite (Py I), reflected light, oil, PPL. Py: pyrite, Cpy: chalcopyrite, Dig: digenite, Cov: covellite.



Figure 12. Photomicrograph of disseminated fine-grained anhedral chalcopyrite in inner parts of altered zones, reflected light, oil, PPL.

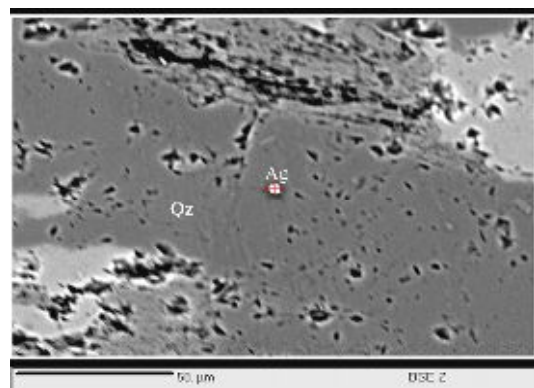


Figure 13. Back-scattered electron image showing close association of native silver (Ag) with siliceous gangue (Qz).

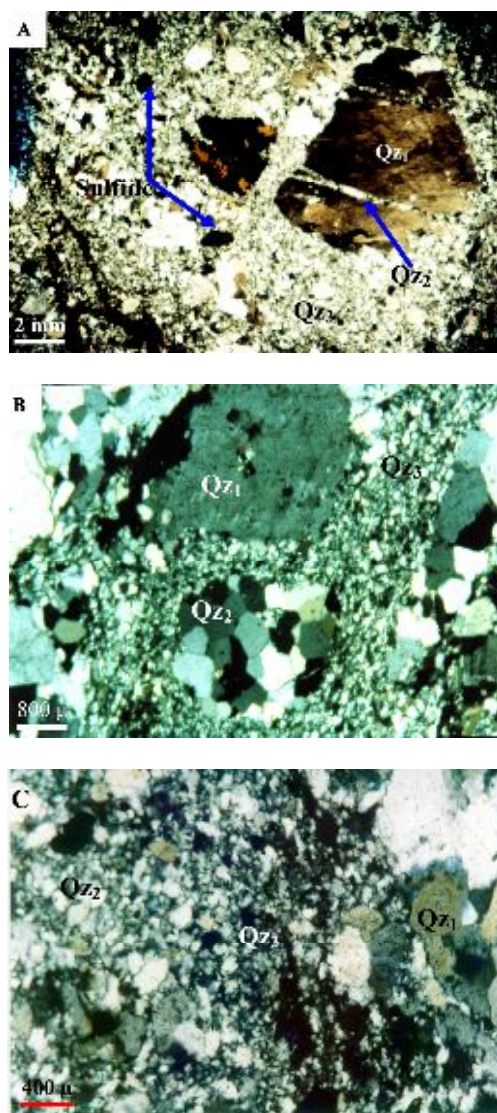


Figure 14. Photomicrographs of three distinct types of quartz in mylonite and ultramylonite zones. A: The pre-deformational quartz (Qz₁) as porphyroblasts which are crosscutting by veinlets of early hydrothermal quartz (Qz₂). B: Recrystallized granular aggregates of the early hydrothermal quartz (Qz₂), C: The late sulfide-bearing quartz (Qz₃) localized around the two previous types and in their microfractures. The black minerals are sulfides. All pictures are in transmitting light, XPL.

Sub-stage II is accompanied by occurrence of siliceous (quartz III) and sulfide (type II) alteration and contains the second and the main phase of gold mineralization in Chah-Bagh. Sulfide alteration is characterized by fine-grained anhedral gold-bearing pyrite and chalcopyrite. These crystals occur as disseminations, vein-veinlets (parallel to or crosscutting the foliation) localized along the weak surfaces of

		Stage I	Stage II	
			Sub-stage I	Sub-stage II
Pyrite	Type I	_____		
	Type II	_____		
Arsenopyrite		_____		
Chalcopyrite	Type I	_____		
	Type II	_____		
Gold		_____		
Silver		_____		
Quartz	Type II	_____		
	Type III	_____		
Textures	Disseminated	_____		
	Laminated	_____		
	Vein & veinlet	_____		

Figure 15. Mineral paragenesis and ore textures at the Chah-Bagh gold occurrence.

previous minerals. The last stage of siliceous alteration (quartz III) belongs to this sub-stage and is characteristically associated with sulfides. The minerals of this phase demonstrated no deformation signature, and probably were deposited late in the hydrothermal and deformation history. Silver occurs as either native Ag associated with quartz or as invisible Ag in sulfide minerals. However, gold occurs only as invisible Au in sulfide minerals.

Conclusions

The mineralogical and geochemical compositions of the ore minerals associated with gold at Chah-Bagh indicate that gold mineralization is associated with sulfide minerals. Two types of sulfide minerals were recognized: 1) the earlier (pyrite I, arsenopyrite and chalcopyrite I) occurs as euhedral to subhedral coarse isolated grains, usually parallel to the mylonitic foliation. The second type (pyrite II and chalcopyrite II) is characterized by disseminations and veinlets of fine grained anhedral to subhedral crystals (parallel to or crosscutting the foliation) localized in Microfractures in previous minerals. There are two phases in the main period of gold mineralization: 1) pyrite I + chalcopyrite I, and 2) pyrite II + chalcopyrite II. Although gold may have been precipitated throughout the hydrothermal alteration process, its precipitation was likely episodic. Pyrite I + chalcopyrite I and pyrite II + chalcopyrite II represent two pulses of gold mineralization, and the precipitation of gold culminated during the formation of the second type of sulfides. The gold grade of ores positively correlates with the sulfide contents, and the

richest ores are those containing fine-grained anhedral pyrite and chalcopyrite. The occurrence of these sulfide minerals (\pm Au) is localized in quartz veins which are parallel to or cut across the dominant foliation (ductile shear deformation). This phenomenon indicates simultaneous precipitation of quartz and sulfides (\pm Au) during the same hydrothermal alteration [42]. Both the ductile and brittle structures hosting gold mineralization are interpreted to have formed within a single, continuous extensional event, which started with ductile deformation and gradually changed into brittle deformation during the late Cretaceous to early Tertiary [27]. Although electron microprobe analyses of auriferous sulfide minerals shows that Au is present in quantities sufficient to explain the bulk gold grades, it seems likely that native gold occurs at Chah-Bagh with irregular distribution or as submicroscopic metallic particles, which was simply not present in our polished sections.

Acknowledgment

The authors are grateful to the Tarbiat Modarres University Grants Commission for research funding. Appreciation is also extended to the Muteh Gold Plant for kindly facilitating laboratory analysis and accommodation. The authors are truly grateful to Dr. Mohajjel for petrofabric and deformation analysis, and Dr. Bouzari for critical reviews and constructive comments. The authors are also grateful to Dr. Mehrabi for a thorough review of the manuscript. The authors also thank editors of journal of sciences for reviews, comments, and editorial improvements.

References

- Alavi M. Tectonics of the Zagros orogenic belt of Iran: New data and interpretations. *Tectonophysics*, **229**: 211-238 (1994).
- Alavi M. Regional stratigraphy of the Zagros fold-thrust belt of Iran and its proforeland evolution. *American J. of Sci.*, **304**: 1-20 (2004).
- Mohajjel M., Fergusson C.L., and Sahandi M.R. Cretaceous-Tertiary convergence and continental collision, Sanandaj-Sirjan zone, western Iran. *J. Asian Earth Sci.*, **21**: 397-412 (2003).
- Berberian M. and King G.C.P. Toward a paleogeography and tectonic evolution of Iran. *Canadian J. of Earth Sci.*, **18**: 210-265 (1981).
- Moritz R. and Ghazban F. Gold mineralisation in the Precambrian basement of the Zagros Belt, Esfahan Province, Iran. *Min. Dep.*, 161-164 (1995).
- Moritz R. and Ghazban F. Geological and fluid inclusion studies in the Muteh gold district, Sanandaj-Sirjan zone, Esfahan Province, Iran. *Schweiz Mineral. Petrogr. Mitt.*, **76**: 85-89 (1996).
- Rashidnejad Omran N. Petrology and geochemistry of metavolcano-sedimentary and plutonic rocks of Muteh area (South Delidjan) with special view to genesis of gold mineralization. Ph.D. *Thesis*, Faculty of Basic Sciences, Tarbiat Modarres University, Iran, 404 p., in Farsi (2001).
- Kouhestani H. Geology, mineralogy, geochemistry and fabric of gold mineralization in Chah-Bagh shear zones at Muteh mining area (southwest of Delidjan, Esfahan province). M.Sc. *Thesis*, Faculty of Basic Sciences, Tarbiat Modarres University, Iran, 222 p., in Farsi (2005).
- Groves D.I., Goldfarb R.J., Gebre-Mariam M., Hagemann S.G., and Robert F. Orogenic gold deposits: a proposed classification in the context of their crustal distribution and relationship to other gold deposit types. *Ore Geol. Rev.*, **13**: 7-27 (1998).
- Groves D.I., Goldfarb R.J., Robert F., and Hart C.J.R. Gold deposits in metamorphic belts: overview of current understanding, outstanding problems, future research and exploration significance. *Econ. Geol.*, **98**: 1-29 (2003).
- Kerrick R., Goldfarb R.J., Groves D.I., and Garwin. The geodynamics of world-class gold deposits: characteristics, space-time distribution and origins. In: Hagemann S.G. and Brown P.E. (Eds.), *Gold in 2000. Rev. in Econ. Geol.*, **13**: 501-551 (2000).
- Bierlein F.P., Christie A.B., and Smith P.K. A comparison of orogenic gold mineralization in central Victoria (Aus.), Western South Island (N.Z.) and Nova Scotia (Can.): implication for variation in the endowment of Paleozoic metamorphic terrains. *Ore Geol. Rev.*, **25**: 125-168 (2004).
- Goldfarb R.J., Nash J.T., and Stoesser J.W. (Eds.), *Geochemical studies in Alaska by the U.S. Geological Survey, U.S. Geol. Surv. Bull.*, 1950, E1-E9 (1989).
- Goldfarb R.J., Groves D.I., and Gardoll S. Orogenic gold and geologic time: a global synthesis. *Ore Geol. Rev.*, **18**: 1-75 (2001).
- Bierlein F.P. and Crowe D.E. Phanerozoic Orogenic lode gold deposits. *Rev. Econ. Geol.*, **13**: 103-139 (2000).
- Bouchot V. and Moritz R. (Eds.), *Ageode-geofrance 3D workshop on Orogenic gold deposits in Europe with emphasis on the Variscides: documents du Bureau Recherches Geologiques et Miniere*, 297, 118 p. (2000).
- Heidari S.M. Mineralogy geochemistry and fabric of gold mineralization in shear zones of Kervian area (southwest Saghez, Kourdestan province). M.Sc. *Thesis*, Faculty of Basic Sciences, Tarbiat Modarres University, Iran, in Farsi (2004).
- Rastgoy-Moghadam G.R. Geology, mineralogy, geochemistry and fabric of gold mineralization in Zartorosht deposit, Sanandaj-Sirjan zone (southwest Sabzevaran). M.Sc. *Thesis*, Faculty of Basic Sciences, Tarbiat Modarres University, Iran, in Farsi (2005).
- Rashidnejad Omran N., Emami M.H., Sabzehei M., Rastad E., Bellon H., and Pique A. Lithostratigraphie et histoire pale'ozoique a pale'ocene des complexes metamorphiques de la region de Muteh, zone de Sanandaj-Sirjan (Iran me'ridional). *C. R. Geoscience*, **334**: 1185-1191 (2002).
- Kouhestani H., Rastad E., and Rashidnejad Omran N. Gold mineralization in ductile and brittle shear zones of Chah-Bagh area, Muteh mining area (southwest Delidjan,

- Esfahan). 22nd Symposium of Geosciences, Geological Survey of Iran, in Farsi (2004).
21. Kouhestani H., Rastad E., Rashidnejad Omran N., and Mohajjel M. The role of deformation and alteration in gold mineralization in Chah-Bagh deposit shear zones. 23rd Symposium of Geosciences, Geological Survey of Iran, in Farsi (2005a).
 22. Kouhestani H., Rashidnejad Omran N., and Rastad E. Geological evolution of major and minor elements and their relationship with gold mineralization in Chah-Bagh shear zone, Muteh Mining district. 23rd Symposium of Geosciences, Geological Survey of Iran, in Farsi (2005b).
 23. Seddigh M. Structural analysis of metamorphic rocks at Muteh area. M.Sc. *Thesis*, Faculty of Basic Science, Tarbiat Modarres University, Iran, 93 p., in Farsi (1999).
 24. Saba A. Structural analysis of syndeformational intrusive bodies in north of Varzaneh (northeast of Golpaygan). M.Sc. *Thesis*, Faculty of Basic Science, Tarbiat Modarres University, Iran, 101 p., in Farsi (1999).
 25. Hasani H., Mohajjel M., and Seddigh M. Structural analysis of metamorphic rocks in Muteh area (east of Golpaygan) and associated gold mineralization. *Amir Kabir*, **50**: 225-233, in Farsi (2001).
 26. Valizadeh M.V. and Cantagrel J.M. Premieres donnees radiometricques (K-Ar et Rb-Sr) sur les micas du complexe magmatique du Mont Alvand, pres Hamadan (Iran occidental). *Comptes Rendus, Academie des Sciences Paris, Serie D*, **28**: 1083-1086 (1975).
 27. Moritz R., Ghazban F., and Singer B.S. Eocene gold ore formation at Muteh, Sanandaj-Sirjan tectonic zone, Western Iran: A result of late-stage extension and exhumation of metamorphic basement rocks within the Zagros Orogen. *Econ. Geol.*, **101**: 1497-1524 (2006).
 28. Arehart G.B., Chryssoulis S.L., and Kesler S.E. Gold and arsenic in iron sulfides from sediment-hosted disseminated gold deposits: Implications for depositional processes. *Ibid.*, **88**: 171-185 (1993).
 29. Dill H.G., Weiser T., Bernhardt I.R., and Kilibarda R.C. The composite gold-antimony vein gold deposit at Kharma (Bolivia). *Ibid.*, **90**: 51-66 (1995).
 30. Fleet M.E., MacLean P.J., and Barbier J. Oscillatory-zoned As-bearing pyrite from stratabound gold deposits: An indication of the fluid evolution. *Econ. Geol. Mon.*, **6**: 356-362 (1989).
 31. Rytuba J. Geochemistry of hydrothermal transport and deposition of gold and sulfide minerals in Carlin-type gold deposit. *U.S. Geol. Surv. Bull.*, **1646**: 27-34 (1985).
 32. Ballantyne J.M., and Moore J.N. Arsenic geochemistry in geothermal systems. *Geochem. Cosmochim. Acta*, **52**: 475-483 (1988).
 33. Pals D.W., Spry P.G., and Chryssoulis S. Invisible gold and tellurium in arsenic-rich pyrite from the Emperor gold deposit, Fiji: implications for gold distribution and deposition. *Econ. Geol.*, **98**: 479-493 (2003).
 34. Clark L.A. The Fe-As-S system: phase relations and applications. *ibid.*, **55**: 1345-1381, 1631-1652 (1960).
 35. Fleet M.E. and Mumin A.H. Gold-bearing arsenian pyrite and marcasite and arsenopyrite from Carlin Trend gold deposits and laboratory synthesis. *Ame. Mineral.*, **82**: 182-193 (1997).
 36. Dickson F.W., Radtke A.S., Geissberg B.G., and Heropoulos C. Solid solutions of antimony, arsenic and gold in stibnite (Sb₂S₃), orpiment (As₂S₃) and realgar (AsS). *Econ. Geol.*, **69**: 591-594 (1974).
 37. Sibson R.H., Robert F., and Poulsen K.H. High-angle reverse faults, fluid-pressure cycling and mesothermal gold-quartz deposits. *Geology*, **16**: 551-555 (1988).
 38. Yardley B.W.D., Rochelle C.A., Barnicoat A.C., and Lloyd G.E. Oscillatory zoning in metamorphic minerals: an indicator of infiltration metasomatism. *Mineral. Mag.*, **55**: 357-365 (1991).
 39. Asadi H.H., Voncken J.H.L., and Hale M. Invisible gold at Zarshuran, Iran. *Econ. Geol.*, **94**: 1367-1374 (1999).
 40. Asadi H.H., Voncken J.H.L., Kuhnelt R.A., and Hale M. Petrography, mineralogy and geochemistry of the Zarshuran Carlin-like gold deposit, northwest Iran. *Mineral. Dep.*, **35**: 656-671 (2000).
 41. Hammond N.Q. and Tabata H. Characteristics of ore minerals associated with gold at the Prestea mine, Ghana. *Min. Mag.*, **61**: 879-894 (1997).
 42. Uemoto T., Ridley J., Mikucki E., Groves D.I., and Kusakabe M. Fluid chemical evolution as a factor in controlling the distribution of gold at the Archean Golden Crown lode gold deposit, Murchison province, Western Australia. *Econ. Geol.*, **97**: 1227-1248 (2002).
 43. Mumin A.H., Fleet M.E., and Chryssoulis S.L. Gold mineralization in As-rich mesothermal gold ores of the Bogosu-Prestea mining district of the Ashanti gold belt, Ghana: Remobilization of invisible gold. *Mineral. Dep.*, **29**: 445-460 (1994).
 44. Michel D., Giuliani G., Olivo G.R., and Marini O.J. As growth banding and the presence of Au in pyrites from the Santa Rita gold vein deposit hosted in Proterozoic metasediments Gaias State, Brazil. *Econ. Geol.*, **89**: 193-200 (1994).
 45. Genkin A.D., Bortnikov N., Cabri L.J., Wagner F.E., Stanley C.J., Safonov Y.G., McMahon G., Friedl J., Kersin A.L., and Gammayanin G.N. A multidisciplinary study of invisible gold in arsenopyrite from four mesothermal gold deposits in Siberia, Russian Federation. *Ibid.*, **93**: 463-487 (1998).
 46. Simon G., Kesler S.E., and Chryssoulis S. Geochemistry and textures of gold-bearing arsenian pyrite, Twin Creeks, Nevada: Implications for deposition of gold in Carlin-type deposits. *Ibid.*, **94**: 405-422 (1999b).
 47. Mehrabi B., Yardley B.W.D., and Cam J.R. Sediment-hosted disseminated gold mineralization at Zarshuran, NW Iran. *Mineral. Dep.*, **34**: 673-696 (1999).
 48. Mohajjel M. Structure and tectonic evolution of Paleozoic-Mesozoic rocks, Sanandaj-Sirjan zone, Western Iran, Ph.D. *Thesis*, Uni. of Wollongong, Australia (1997).